A&A manuscript no.
(will be inserted by hand later)

Your thesaurus codes are:
01(02.01.4; 02.12.1; 03.20.8; 11.17.1; 11.17.4 IRAS 13349+2438; 13.25.2)

ASTRONOMY AND ASTROPHYSICS
October 1, 2000

Complex resonance absorption structure in the X-ray spectrum of IRAS 13349+2438*

M. Sako[1], S. M. Kahn[1], E. Behar[1], J. S. Kaastra[2], A. C. Brinkman[2], Th. Boller[3], E. M. Puchnarewicz[4], R. Starling[4], D. A. Liedahl[5], J. Clavel[6], and M. Santos[6]

[1] Department of Physics and Columbia Astrophysics Laboratory, 550 West 120th Street, New York, NY 10027, USA
[2] Space Research Organization of the Netherlands, Sorbonnelaan 2, 3548 CA, Utrecht, The Netherlands
[3] Max-Planck-Institut fuer Extraterrestrische Physik, Postfach 1603, 85741 Garching, Germany
[4] Mullard Space Science Laboratory, University College, London, Holmbury St. Mary, Dorking, Surrey, RH5 6NT, UK
[5] Physics Department, Lawrence Livermore National Laboratory, P.O. Box 808, L-41, Livermore, CA 94550
[6] XMM Science Operations, Astrophysics Division, ESA Space Science Dept., P.O. Box 50727, 28080 Madrid, Spain

Received 29 September 2000 / Accepted

Abstract. The luminous infrared-loud quasar IRAS 13349+2438 was observed with the *XMM-Newton* Observatory as part of the Performance Verification program. The spectrum obtained by the Reflection Grating Spectrometer (RGS) exhibits broad ($FWHM \sim 1400$ km s^{-1}) absorption lines from highly ionized elements including hydrogen- and helium-like carbon, nitrogen, oxygen, and neon, and several iron L-shell ions (Fe XVII – XX). Also shown in the spectrum is the first astrophysical detection of a broad absorption feature around $\lambda = 16 - 17$ Å identified as an unresolved transition array (UTA) of $2p - 3d$ inner-shell absorption by iron M-shell ions in a much cooler medium; a feature that might be misidentified as an O VII edge when observed with moderate resolution spectrometers. No absorption edges are clearly detected in the spectrum. We demonstrate that the RGS spectrum of IRAS 13349+2438 exhibits absorption lines from two distinct regions, one of which is tentatively associated with the medium that produces the optical/UV reddening.

Key words: atomic processes – line: formation – techniques: spectroscopic – quasars: absorption lines – quasars: individual: IRAS 13349+2438 – X-rays: galaxies

1. Introduction

IRAS 13349+2438 is an archetypal highly-polarized radio-quiet quasar at a redshift of $z = 0.10764$ (Kim et al. 1995). Since its identification as an infrared-luminous quasar (Beichman et al. 1986), this source has been extensively studied in the optical, infrared, and X-ray bands. In a detailed investigation of the optical and infrared spectra and polarization measurements, Wills et al. (1992) demonstrated that the nuclear spectrum exhibits two distinct components; a highly-reddened component and a highly-polarized component that suffers much lower extinction. Based on these observational facts, Wills (1992) constructed a simple and elegant picture of the nuclear region of IRAS 13349+2438 in which the direct AGN radiation is attenutated through a thick dusty torus, while the observed highly-polarized light is produced by scattering in an extended bipolar region, either by warm electrons or by small dust grains.

IRAS 13349+2438 was detected in the *ROSAT* All-Sky-Survey (Walter & Fink 1993; Brinkmann & Siebert 1994), and has been the target of extended pointed observations with *ROSAT* (Brandt, Fabian, & Pounds 1996), and with *ASCA* (Brinkmann et al. 1996; Brandt et al. 1997). In general, the analyses of these data sets have suggested the presence of absorption edge features due to ionized species of oxygen (O VIII and O VII), although, because of the low spectral-resolving-power capabilities of the available detectors on these missions, the precise nature of the soft X-ray spectrum has remained controversial. Siebert & Brinkmann (1999) self-consistently accounted for the effects of dust embedded in the warm absorbing medium, and concluded that single zone models, both with and without internal dust, do not provide adequate fits to the combined, *ROSAT*, *ASCA*, and optical data sets. In particular, they find that a dust-free warm absorber model formally gives the best fit to the X-ray data, and conclude that the X-ray absorption and optical reddening must arise in spatially distinct regions.

In this Letter, we present results from the first high-resolution X-ray observation of IRAS 13349+2438 with the *XMM-Newton* Observatory. The spectrum obtained with the Reflection Grating Spectrometer (RGS) shows a wealth of discrete spectral features, including the first

* Based on observations obtained with *XMM-Newton*, an ESA science mission with instruments and contributions directly funded by ESA Member States and the USA (NASA).

astrophysical detection of inner-shell $2p - 3d$ absorption by M-shell iron ions in the form of an unresolved transition array (UTA). From a detailed analysis of the rich absorption spectrum, we measure the column density and velocity field of the line-of-sight material. We show that the spectrum contains absorption features from regions with two distinct levels of ionization. The column density of the lower ionization component is consistent with the observed optical reddening, and we tentatively associate this component with the dusty torus.

2. Observation and Data Reduction

IRAS 13349+2438 was observed with the *XMM-Newton* observatory (Jansen et al. 2000) on 19 – 20 June, 2000 during the Performance Verification phase for a total exposure time of 42 ks. The data obtained with the RGS (den Herder et al. 2000) were filtered through standard event-selection criteria using the *XMM-Newton* Science Analysis Software (SAS). The source spectrum was extracted using both dispersion/cross-dispersion coordinates and dispersion/pulse-height coordinates, which include 90% of the source photons. The background spectrum was generated using all of the events that lie outside the spatial mask. Wavelengths were then assigned to the dispersion coordinates. The current wavelength scale is accurate to within ~ 8 mÅ across the entire RGS band of $\lambda = 5-35$ Å ($E = 0.35 - 2.5$ keV).

The European Photon Imaging Camera (EPIC; Turner et al. 2000) MOS1 data were also processed with the SAS. The MOS2 detector was operated in FAST UNCOMP mode, for which reduction by the SAS is not possible as yet. Source events were extracted using a circular region of radius 45″. A nearby source-free region with a radius of 3′ was used for the background.

Three modes of the Optical Monitor (OM; Mason et al. 2000) were used during the observation. The V grism (or optical grism; exposure time 3000 s), UV grism (exposure time 1000 s), and the UVW2 filter ($\sim 1500 - 3000$ Å; effective exposure time 6340 s). There is no significant variability in the UVW2 observations. Absolute flux calibrations for the grism data were not available at the time of writing. The optical spectrum shows clear evidence of Hβ emission but the signal-to-noise is insufficient to determine the presence of any other emission lines (within an observer frame wavelength range of $\sim 3000 - 6000$ Å). The UV spectrum (coverage $\sim 2000 - 3500$ Å) is too weak for spectral extraction.

3. Results of Spectral Fitting

3.1. Underlying Continuum Radiation

To first obtain a rough characterization of the shape of the continuum, we use the EPIC-PN spectrum, which has the highest statistical quality and covers a broad range in energy. The $0.2 - 10$ keV spectral region can be well-fitted

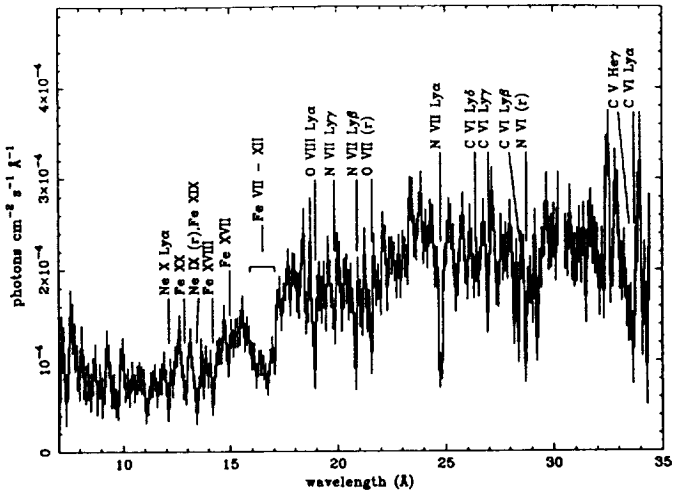

Fig. 1. The RGS first order spectrum of IRAS 13349+2438 corrected for cosmological redshift ($z = 0.10764$). The error bars represent 1σ Poisson fluctuations.

with a phenomenological model that consists of a power-law and two black body components absorbed through a Galactic column density of $N_{\rm H}^{\rm gal} = 1.1 \times 10^{20}$ cm^{-2} (Murphy et al. 1996). The EPIC-PN data require two black body components with temperatures of $kT \sim 70$ eV and ~ 12 eV. The best-fit powerlaw photon index of $\Gamma \sim 2.2$ is consistent with the value implied by the *ASCA* data (Brinkmann et al. 1996; Brandt et al. 1997).

The MOS1 data from 0.3 to 10 keV, excluding the $0.6 - 1.2$ keV region where the RGS shows complex absorption features, were best-fit using a single blackbody plus power-law (a χ^2_r of 1.59 for 199 degrees of freedom), which is generally consistent with the PN data. The blackbody temperature is $kT \sim 110$ eV. The best-fit photon index is $\Gamma = 2.1$ with a column density of 1.4×10^{20} cm^{-2}, which is only slightly higher than the Galactic value of 1×10^{20} cm^{-2}.

3.2. The Absorption Spectrum of IRAS 13349+2438

The RGS spectrum shown in Figure 1 exhibits numerous absorption lines from a wide range in levels of ionization. The most prominent features in the spectrum are K-shell absorption lines of H- and He-like carbon, nitrogen, oxygen, and neon, and L-shell lines of Fe XVII – XX. The spectrum also shows a broad absorption feature between $\lambda \sim 16 - 17$ Å ($E \sim 730 - 770$ eV). The observed location of the red "edge" of this feature is at $\lambda = 17.10 \pm 0.05$ Å in the rest-frame of the quasar, and is close but undoubtedly inconsistent with that of the O VII photoelectric edge ($\lambda = 16.78$ Å). The shape of the absorption trough towards the shorter wavelengths is also incompatible with that of a photoelectric edge. We identify this feature as a UTA of inner-shell $2p - 3d$ resonance absorption lines in relatively cool, M-shell iron. The shape of this feature is strikingly similar to laboratory absorption measurements

of a heated iron foil (Chenais-Popovics et al. 2000), and also agrees well with our own calculations as described below.

We adopt a continuum model similar to that inferred from the EPIC-PN data; i.e., the sum of a powerlaw and a blackbody component, the latter merely in order to parametrize empirically the soft X-ray spectral shape. We also fix the powerlaw photon index to $\Gamma = 2.2$ and the column density of cold material to the Galactic value. With the continuum model defined, we then apply absorption components of H- and He-like C, N, O, and Ne, and Fe XVII – XXIV. Each ion is treated as a separate component in the spectral fit and contains all relevant resonance transtions from the ground-state and photoelectric edges in the RGS band. The line profiles are calculated accounting for thermal and turbulent velocity broadening. Transition wavelengths and oscillator strengths of the upper levels were calculated with the atomic physics package HULLAC (Bar-Shalom et al. 1998), except for the wavelengths of the strong Fe L resonance lines where we use laboratory measurement values described in Brown et al. (2000). We use photoionization cross sections from Verner et al. (1996). For the iron UTA absorption, photon impact processes involving L-shell to M-shell excitations in Fe V – XVI are computed. All of the transitions $2l^8\ 3l^x$ - $2l^7\ 3l^{x+1}$ (x = 1 through 12) are taken into account, of which the 2p - 3d excitations are the most important. For the atomic structure, the most significant configuration mixings, which conserve the total angular momentum within the $n = 3$ shell (namely $3p^2 + 3s3d$), are included. This approximation is expected to be adequate for analysing the presently observed unresolved absorption feature. A more detailed discussion of the UTA is presented in Behar, Sako, & Kahn (2000).

Each component is then fit for the ion column density simultaneously with the black body continuum parameters and the normalization of the powerlaw component. The best-fit black body temperature is $kT \sim 100$ eV with a flux in the 5 – 35 Å range of 4.0×10^{-3} photons cm^{-2} s^{-1}. The flux in the powerlaw component is 2.4×10^{-3} photons cm^{-2} s^{-1} in the same wavelength range.

The observed widths of the absorption lines, as shown below, are much larger than both the instrument line spread function and the thermal broadening of a gas with $kT \sim 10$ eV, which is the expected temperature for a photoionized plasma at this level of ionization. With the current statistical quality of the RGS data, however, we are not able to constrain the turbulent velocities $v_{\rm turb}$ of the individual ion components. We, therefore, assume a uniform mean turbulent velocity field, keeping in mind that each ion can, in principle, exist in regions of different turbulent velocities. The derived ion column densities, therefore, may be uncertain to some degree, as quantified in the following section.

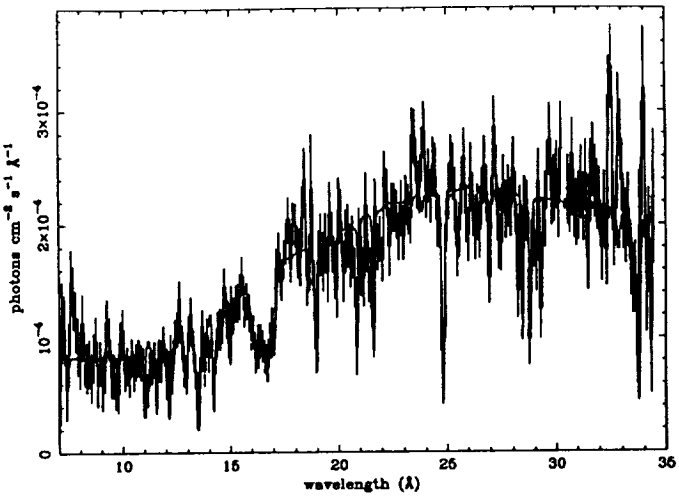

Fig. 2. Same as in Figure 1 with the best-fit model spectrum superimposed.

We obtain a statistically acceptable fit to the RGS data with $\chi^2_r = 1.07$ for 532 degrees of freedom. The continuum parameters inferred from the RGS data are also consistent with those derived from EPIC-PN and EPIC-MOS. The intrinsic isotropic luminosities in the 0.3 – 2 keV and 2 – 10 keV regions are $L_X \sim 2 \times 10^{44}$ erg s^{-1} and $\sim 5 \times 10^{43}$ erg s^{-1} (assuming $H_0 = 65$ km s^{-1} Mpc^{-1} and $q_0 = 0.5$), respectively, which are lower than both the *ROSAT* PSPC and *ASCA* values by a factor of ~ 5. The measured ion column densities are listed in Table 1. To illustrate the statistical significance of the various components, we also list the changes in χ^2 when each of the components is removed from the model. The best-fit *FWHM* turbulent velocity is $v_{\rm turb} = 1430^{+360}_{-280}$ km s^{-1}, which is much larger than the thermal velocity of a photoionized medium. We also find weak evidence of an average bulk outflow velocity shift with $v_{\rm shift} = +200^{+170}_{-180}$ km s^{-1}, where positive velocity denotes a blueshift.

4. Implications of the Results of Spectral Fitting

For the measured ion column densities listed in Table 1, many of the strong absorption lines of neon and iron L ions are in the logarithmic region of the curves of growth, which indicates that the derived column densities are highly coupled with the assumed turbulent velocity. Those of K-shell carbon, nitrogen, and oxygen, and iron M-shell ions, however, are in the linear regime, and the derived column densities are not very sensitive to the turbulent velocity.

As shown in Table 1, the detections of absorption lines from Fe VII – XII and Fe XVII – XX are highly significant. The column densities of the intermediate charge states of Fe XIII – XVI, however, are consistent with zero. This indicates that the line-of-sight material consists of either a multi-phase gas in a single medium, or two (or more) spatially distinct regions. Motivated by this observational fact, we refit the spectrum using the same model, ex-

Table 1. Measured Ion Column Densities

Ion	N_i (cm^{-2}) [a]	$\Delta\chi^2$ [b]
C V	$(6.3^{+5.2}_{-4.8}) \times 10^{16}$	4.8
C VI	$(6.0^{+6.4}_{-3.1}) \times 10^{16}$	23.7
N VI	$(2.4^{+1.4}_{-1.0}) \times 10^{16}$	29.1
N VII	$(1.3^{+0.8}_{-0.4}) \times 10^{17}$	109.5
O VII	$(3.7^{+2.7}_{-1.8}) \times 10^{16}$	24.2
O VIII	$(9.5^{+8.7}_{-4.7}) \times 10^{16}$	24.7
Ne IX	$(1.2^{+0.6}_{-0.5}) \times 10^{18}$	9.9
Ne X	$(4.9^{+10}_{-3.2}) \times 10^{17}$	25.9
Fe XVII	$(1.7^{+1.6}_{-1.2}) \times 10^{17}$	23.0
Fe XVIII	$(6.3^{+2.4}_{-1.9}) \times 10^{17}$	115.0
Fe XIX	$(9.7^{+4.8}_{-3.9}) \times 10^{17}$	166.7
Fe XX	$(3.0^{+2.8}_{-2.0}) \times 10^{17}$	39.5
Fe VII	$(1.5^{+1.5}_{-1.3}) \times 10^{16}$	9.6
Fe VIII	$(4.6^{+1.5}_{-1.3}) \times 10^{16}$	91.8
Fe IX	$(8.8^{+12}_{-8.7}) \times 10^{15}$	29.3
Fe X	$(2.4^{+1.3}_{-1.1}) \times 10^{16}$	72.4
Fe XI	$(1.9^{+1.1}_{-0.9}) \times 10^{16}$	65.3
Fe XII	$(6.4^{+10}_{-4.4}) \times 10^{16}$	25.6

[a] The turbulent velocities for all of the ions are fixed to the same value. We find a best-fit with $v_{\rm turb} = 1430^{+360}_{-280}$ km s^{-1} *FWHM*.
[b] The increase in χ^2 when the ion component is excluded from the best-fit model.

cept, we assume that the line-of-sight material consists of two discrete velocity components; (1) the low-ionization-parameter component including C VI, C V, N VI, O VII, and the M-shell Fe, and (2) the high-ionization-parameter component including N VII, O VIII, Ne IX, Ne X, and L-shell Fe. Contrary to our previous fit where the bulk velocities of all the ions were fixed relative to one another, we find that the low-ionization-parameter component is significantly blue-shifted with $v_{\rm shift,low} = +420^{+190}_{-180}$ km s^{-1}, while the bulk velocity shift in the high-ionization component is consistent with zero ($v_{\rm shift,high} = -20^{+200}_{-330}$ km s^{-1}). This implies that the low-ionization gas is being accelerated substantially compared to the high-ionization component, as would be expected in a radiatively-driven outflow (Arav & Li 1994). The derived turbulent velocities of both components remain consistent with that of our previous fit ($v_{\rm turb,FWHM} \sim 1500$ km s^{-1}).

From the observed distribution of charge states of M-shell iron, the average ionization parameter, $\xi = L/nr^2$, of the absorbing gas is estimated to be $\log\xi \sim 0$ based on a calculation with the photoionization code XSTAR (Kallman & Krolik 1995) using the inferred continuum shape for the illuminating spectrum. The measured ion column densities suggest that the corresponding equivalent hydrogen column density is $N_{\rm H} \sim 2 \times 10^{21}$ cm^{-2} assuming a solar iron abundance. This low-ξ gas accounts for most of the carbon and He-like nitrogen and oxygen absorption lines as well. The lack of absorption from Fe XIII – XVI, however, indicates that substantial amounts of material with ionization parameters in the range $1 \lesssim \log\xi \lesssim 2$ are not present along the line-of-sight. Whether this is related to the global structure of the circumnuclear medium or a mere coincidence from a superposition of physically distinct regions is not known.

The absorption lines from H-like nitrogen and oxygen, H- and He-like neon, and L-shell iron are produced in a medium with $2.0 \lesssim \log\xi \lesssim 2.5$ and an equivalent hydrogen column density of $N_{\rm H} \sim 1 \times 10^{22}$ cm^{-2}. For a normal dust-to-gas ratio, the observed reddening of $E(B-V) = 0.3$ (Wills et al. 1992) corresponds to a hydrogen column density of $N_{\rm H} = 1.7 \times 10^{21}$ cm^{-2} (Burstein & Heiles 1978). This value is slightly lower than the total amount of X-ray absorbing material observed in the present X-ray spectrum. Coincidentally, however, the derived column density of the low-ξ component is very close to that of the optical reddening, although, we cannot conclusively associate the low-ξ X-ray absorber with the dusty torus. The column density of the high-ξ component, on the other hand, is a factor of ~ 5 higher.

An interesting point to note is that the $1 \lesssim \log\xi \lesssim 2$ region is *not* thermally unstable, based on XSTAR calculations described above. On the other hand, the high-ξ region ($2.0 \lesssim \log\xi \lesssim 2.5$) that we observe in the spectrum *is* thermally unstable. However, complications such as non-solar metal abundances and/or inaccurate ionization and recombination rates may alter the shape of the thermal stability curve significantly, and, hence, the temperature ranges of the unstable regions (Hess, Kahn, & Paerels 1997; Savin et al. 1999).

5. Comparisons with Other AGNs

The absorption spectrum of IRAS 13349+2438 is qualitatively similar to those obtained with the *Chandra* transmission grating observations of the Seyfert 1 galaxies NGC 5548 and NGC 3783, which show narrow resonance absorption lines blue-shifted by several hundred km s^{-1}. (Kaastra et al. 2000; Kaspi et al. 2000). The derived ion column densities in these sources, as well as in IRAS 13349+2438, are in the range $N_i \sim 10^{16}-10^{17}$ cm^{-2}, and are not high enough to produce observable absorption edges.

Conceptually, the low-ionization component observed in IRAS 13349+2438 is similar to the "lukewarm absorber" that explains both the observed optical and X-ray attenuation in NGC 3227 (Kraemer et al. 2000). The spectroscopic signatures, however, are very different. In particular, for the column densities derived from the IRAS 13349+2438 data, the absorption features are dominated by discrete resonance line transitions, mainly in He-like ions and M-shell iron, and not by photoelectric edges as in the model of Kraemer et al. (2000).

As demonstrated in our detailed spectral analysis of IRAS 13349+2438, the UTA feature is potentially a powerful diagnostic tool for probing cool absorbing material using high-resolution X-ray observations. If the low-ionization component is indeed associated with the dusty torus as the derived column density suggests, this feature should be detectable in other AGNs where the line-of-sight is partially obscured by the torus.

Acknowledgements. The Columbia University team is supported by NASA. The Laboratory for Space Research Utrecht is supported financially by the Netherlands Organization for Scientific Research (NWO).

References

Arav, N., & Li, Z.-Y. 1994, ApJ, 427, 700
Bar-Shalom, A., Klapisch, M., Goldstein, W. H., & Oreg, J. 1998, the HULLAC code for atomic physics (unpublished)
Behar, E., Sako, M., & Kahn, S. M. 2000, in preparation
Beichman, C. A., Soifer, B. T., Helou, G., Chester, T. J., Neugebauer, G., Gillet, F. C., & Low, F. J. 1986, ApJ, 308, L1
Boroson, T. A., & Meyers, K. A. 1992, ApJ, 397, 442
Brandt, W. N., Fabian, A. C., & Pounds, K. A. 1996, MNRAS, 278, 326
Brandt, W. N., Mathur, S., Reynolds, C. S., & Elvis, M. 1997, MNRAS, 292, 407
Brinkmann, W., Kawai, N., Ogasaka, Y., & Siebert, J. 1996, A&A, 316, L9
Brinkmann, W., & Siebert, J. 1994, A&A, 285, 812
Brown, G.V., Beiersdorfer, P., Liedahl, D.A., Widmann, K., & Kahn, S.M. 2000, LLNL preprint (UCRL-JC-136647)
Burstein, D., & Heiles C. 1978, ApJ, 225, 40
Chenais-Popovics, C., et al. 2000, ApJS, 127, 275
den Herder, J. W., et al. 2000, this issue
Hess, C. J., Kahn, S. M., & Paerels, F. B. S. 1997, ApJ, 478, 94
Jansen, F. A., et al. 2000, this issue
Kaastra, J. S., Mewe, R., Liedahl, D. A., Komossa, S., & Brinkman, A. C. 2000, A&A, 354, L83
Kallman, T. R., & Krolik, J. H. 1995, XSTAR – A Spectral Analysis Tool, HEASARC (NASA/GSFC, Greenbelt)
Kaspi, S., Brandt, W. N., Netzer, H. Sambruna, R., Chartas, G., Garmire, G., & Nousek, J. A. 2000, ApJ, 535, L17
Kim, D.-C., Sanders, D. B., Veilleux, S., Mazzarella, J. M., & Soifer, B. T. 1995, ApJS, 98, 129
Kraemer, S. B., George, I. M., Turner, T. J., & Crenshaw, D. M. 2000, ApJ, 535, 53
Mason, K., et al. 2000, this issue
Murphy, E. M., Lockman, F. J., Laor, A., & Elvis, M. 1996, ApJS, 105, 369
Savin, D. W., et al. 1999, ApJS, 123, 687
Siebert, J., Komossa, S., & Brinkmann, W. 1999, A&A, 351, 893
Turner, M., et al. 2000, this issue
Verner, D. A., Ferland, G. J., Korista, K. T., & Yakovlev, D. G. 1996, ApJ, 465, 487
Walter, R., & Fink, H. H. 1993, A&A, 274, 105
Wills, B. J., Wills, D., Evans, N. J., Natta, A., Thompson, K. L., Breger, M., & Sitko, M. L. 1992, ApJ, 400, 96